Energy Conversion and Management 89 (2015) 683–689

Contents lists available at ScienceDirect

Energy Conversion and Management

journal homepage: www.elsevier.com/locate/enconman

Performance characteristics of a direct carbon fuel cell/thermoelectric generator hybrid system

Mingzhou Zhao [a], Houcheng Zhang [a,*], Ziyang Hu [a], Zhufeng Zhang [b], Jinjie Zhang [c]

[a] Department of Microelectronic Science and Engineering, Ningbo University, Ningbo 315211, China
[b] Department of Physics, Ningbo University, Ningbo 315211, China
[c] School of Marine Science, Ningbo University, Ningbo 315211, China

ARTICLE INFO

Article history:
Received 7 August 2014
Accepted 15 October 2014

Keywords:
Direct carbon fuel cell
Thermoelectric generator
Hybrid system
Irreversibility
Performance characteristic

ABSTRACT

A hybrid system mainly composed of a DCFC (Direct Carbon Fuel Cell), a TEG (Thermoelectric Generator) and a regenerator is put forward, where the DCFC electrochemically converts the chemical energy in the solid carbon into electricity and waste heat, and the TEG further converts the waste heat into electricity for additional power generation. The main irreversibilities in each element of the hybrid system are characterized, and the heat losses between the DCFC and the environment are also considered. Numerical expressions for the power output and efficiency of the hybrid system are respectively derived, from which the general performance characteristics are revealed. The fundamental relationship between the operating current density of the DCFC and the dimensionless electrical current of the TEG is obtained, and thus the region of the operating current density of the DCFC that the TEG exerts its function is determined. By using such a system, the equivalent maximum power density of the hybrid system allows to be 50% larger than that of the sole DCFC system. The effects of the operating current density, operating temperature, heat conductivity, and some integrated parameters on the performance of the hybrid system are discussed.

1. Introduction

The worldwide growing demand for electrical energy cannot be compensated by renewable energies in the medium term [1]. Coal is the most abundant and economic fossil resource on the earth and is forecast to account for 28% of the word's increased primary energy consumption by 2030 [2]. Therefore, the development and deployment of clean coal technologies are crucial to promote sustainable development [3]. A promising development in this context could be direct carbon fuel cell (DCFC) that has the potential to directly convert the chemical energy in solid carbon into electricity without the need for gasification or the moving machinery associated with conventional electric generators. DCFCs offer comparative high efficiency of conversion and can yield 2–3 times the amount of electrical energy as coal-fired power plants for a given amount of carbon, resulting in a 50% reduction in carbon dioxide emissions per unit of electricity generation [4]. DCFCs can use coal coke, petroleum coke, and gas carbon as well as biomass carbon as fuel, and the exhaust gas is an almost CO_2 stream [5,6]. The nearly pure CO_2 stream can be easily collected for downstream disposal using methods such as carbon sequestration, and thereby, the energy and cost penalties to capture the CO_2 will also be significantly less than other technologies [7].

However, one of the major drawbacks of DCFCs that prohibits its commercialization stage is its comparative low power density [7]. The maximum power density obtained from DCFCs has undergone many advances in recent years not only due to the progresses in the materials fabrication but also due to the optimized operating conditions and DCFC system design [8–14]. As an alternative approach, the equivalent maximum power density of DCFC can be also effectively elevated by employing cogeneration systems [15–17]. Steinberg [15] developed a high efficiency energy cycle by integrating a molten carbonate DCFC with a hydrogen plasma black reactor (HPBR) to convert the fossil and biomass fuels to electric power and transportation fuels, it was found that the overall thermal efficiency for electricity and hydrogen or transportation fuel was estimated to vary from 70% to 90%. Liu et al. [16] built and simulated a highly efficient energy system mainly composed of a methane catalytic decomposition reactor (MCDR), a DCFC, an internal reforming solid oxide fuel cell (IRSOFC) and two gas turbines. They found that the DCFC had better high-load performance, while the IRSOFC performed better at relatively lower loads, and 80% of the CO_2 emission was reduced compared to a system

* Corresponding author. Tel.: +86 574 87600770; fax: +86 574 87600744.
E-mail address: zhanghoucheng@nbu.edu.cn (H. Zhang).

http://dx.doi.org/10.1016/j.enconman.2014.10.035
0196-8904/

utilizing a single SOFC. Their further studies showed that the electrical exergy efficiency of 68.24% for the system was achieved and the combined power-heat exergy efficiency could be over 80% if the waste heat in the exhaust was recovered [17].

TEG (Thermoelectric Generator) can directly convert thermal energy into electricity via the Seebeck effect; that is, when a temperature difference is created across the thermoelectric device and an external load is properly connected, a direct-current voltage develops in the thermoelectric elements and electrical current flows through the load [18,19]. Compared with conventional electric power generators, TEG offers many advantages such as being highly reliable, having no moving parts, and being environmentally friendly [20]. There is a growing interest for waste heat recovery TEG using various heat sources such as combustion of solid waste, geothermal energy, power plants, and other industrial heat-generating processes [21–23]. When a DCFC is put into operation, a great part of chemical energy in the fuel will be finally released as waste heat due to the Joule effect of the equivalent internal resistance. Obviously, the waste heat generated in the DCFC can be readily converted into power generation through a bottoming TEG and thus the performance of the DCFC can be effectively enhanced.

In this work, a hybrid system consisting of a DCFC, a TEG and a regenerator is proposed to recover the waste heat generated in the DCFC. The performance parameters of the hybrid system are analytically derived by considering the main irreversible losses in each element of the system. The effectiveness of the hybrid system will be shown by some numerical calculation examples, and the effects of some operating conditions and designing parameters on the performance of the hybrid system will be revealed.

2. A DCFC–TEG hybrid system

The hybrid system presented here consists of a DCFC, a TEG and a regenerator, as schematically shown in Fig. 1, where the TEG is operated between the heat source (i.e., the DCFC) at temperature T and the heat sink (i.e., the environment) at temperature T_0, q_1 and q_2 are respectively the rate of heat input from the DCFC to the thermoelectric generator and the rate of heat rejection from the thermoelectric generator to the environment, q_L is the rate of heat loss between the DCFC and the environment, P_{DCFC} and P_{TEG} are respectively the electrical power outputs of the DCFC and TEG. In this hybrid system, the DCFC not only works as an electrochemical power generator but also acts as the high-temperature heat reservoir of the TEG which generates some additional electricity, and the regenerator is applied to preheat the incoming fuel and oxidant with the comparative high-temperature exhaust product from the DCFC. Employing such a hybrid system, the heat produced in the DCFC can be effectively harvested, and consequently, the performance of the DCFC can be improved.

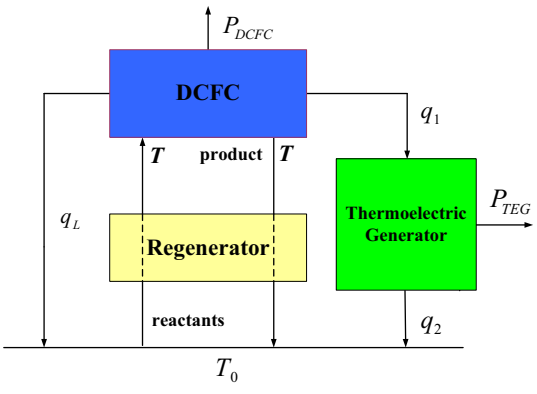

Fig. 1. The schematic diagram of a DCFC–TEG hybrid system.

The whole hybrid system is formulated based on the following general simplifications and assumptions [24–28]:

(1) Both the DCFC and the TEG are operated under steady-state conditions.
(2) Geometric configuration of the TEG is in the optimum form.
(3) Operating temperature and pressure are uniform and constant in the DCFC.
(4) Complete chemical reactions are considered and no reactant is left after the reactions [27].
(5) All gases involved are assumed to be compressible ideal gases.
(6) Carbon fuel is regarded as a rigid sphere and packed with a simple hexagonal pattern.
(7) Carbon fuel is assumed to be oxidized by completely electrochemical reactions.
(8) Heat leakage through the TEG surroundings is neglected.

Based on the above simplifications and assumptions, each component in the hybrid system will be analyzed, and then the performance characteristics of the hybrid system will be synthetically investigated.

2.1. The DCFC

The DCFC directly converts the chemical energy of the incoming graphite into electricity and heat without any gasification, it is mainly composed of a packed bed anode and a lithium doped NiO cathode with Li_2CO_3/K_2CO_3 eutectic melt as an electrolyte sandwiched between the two electrodes. The overall electrochemical reaction proceeded in a DCFC can be summarized as $C + O_2 \rightarrow CO_2$ + Electricity + Heat, electrons are drawn from the anode to the cathode through an external circuit and a direct electric current is produced. As previously described in Ref. [25], the output cell voltage of a DCFC, V, is always lower than the OCV (open circuit voltage), E, because there are some voltage losses resulting from the electrode kinetics, electronic/ionic resistances of the cell components, and reactants/product transportation, which correspond to the activation overpotential (V_{act}), ohmic overpotential (V_{ohm}), and concentration overpotential (V_{con}), respectively. Taking these three losses into account, one may obtain the output cell voltage, power output, and efficiency of a DCFC at certain operating current density

$$V = E - V_{act,a} - V_{act,c} - V_{con} - V_{ohm}, \quad (1)$$

$$P_{DCFC} = VI = VJA, \quad (2)$$

and

$$\eta_{DCFC} = \frac{P}{-\Delta \dot{H}} = -\frac{n_e F V}{\Delta h}, \quad (3)$$

where $E = E_0 + \frac{RT}{n_e F} \ln\left[p_{O_2,cat}(p_{CO_2,cat})^2 p_{CO_2,an}^{-1}\right]$ is the OCV, $E_0 = -\Delta g^0(T)/(n_e F)$, E_0 and $\Delta g^0(T)$ are, respectively, the reversible potential and the Gibbs free energy change at the standard pressure (1 atm) and temperature T, n_e is the number of electrons involved per reaction, R is the universal gas constant, p_{O_2} and p_{CO_2} are, respectively, the partial pressures of O_2 and CO_2 at the electrode surfaces, and the subscripts "*an*" and "*cat*" represent anode and cathode, respectively; $V_{act,m} = \frac{RT}{2F} \ln\left\{J/(2J_{0,m}) + \sqrt{[J/(2J_{0,m})]^2 + 1}\right\}$ is the activation overpotential, I and J are respectively the electric current and operating current density of the DCFC, the subscript "*m*" stands for "*an*" or "*cat*", $J_{0,an} = K_B \exp(-E_B/T)$ and $J_{0,cat} = J^0_{0,cat}(p_{CO_2,cat})^{r_1}(p_{O_2,cat})^{r_2}$ are

respectively the anode exchange current density and the cathode exchange current density [29,30]; $V_{con} = \frac{RT}{n_eF}\ln[J_{\lim}/(J_{\lim} - J)]$ is the concentration overpotential, $J_{\lim} = n_eFK_{CO_2}C^b_{CO_2}$ is the limiting current density, K_{CO_2} is the mass transportation coefficient of CO_2, and $C^b_{CO_2}$ is the concentration of CO_2 in the bulk [24,31]; $V_{ohm} = \sum I_{c,i}R_{c,i} + \sum I_{e,i}R_{e,i} + V_{ec}$ is the ohmic overpotential, $I_{c,i}$ and $I_{e,i}$ are respectively the electric currents flowing through the carbon phase and electrolyte phase at the ith slab in the anode, $R_{c,i}$ and $R_{e,i}$ are respectively the resistances in the carbon phase and electrolyte phase at the ith slab in the anode, V_{ec} is the total ohmic overpotenial in the electrolyte and the cathode [25]; $-\Delta\dot{H} = -\frac{\Delta h}{n_eF}JA$ is the total chemical energy released per unit time, $(-\Delta h)$ is the molar enthalpy change of the electrochemical reaction [25], A is the polar plate area of the DCFC.

2.2. The regenerator

The regenerator in the hybrid system functions as a counter-flow heat exchanger, which heats the incoming reactants from the ambient temperature to the operating temperature of DCFC by absorbing the comparative high-temperature heat contained in the product. Owing to the existence of thermal resistance, some regenerative losses are inevitable and some additional heat from the DCFC should be transferred to compensate the regenerative losses immediately. Assuming the rate of the regenerative losses is proportional to the temperature difference between the DCFC and the environment, the regenerative losses is given by [32,33]

$$q_{re} = \alpha_{re}A_{re}(1-\varepsilon)(T - T_0), \tag{4}$$

where α_{re} and A_{re} are the heat-transfer coefficient and heat-transfer area of the regenerator, respectively.

2.3. The TEG

As show in Fig. 2, the TEG in the hybrid system is closely attached to the DCFC, it is composed of many n- and p-type semiconductor legs that are connected electrically in series by metal strips and thermally in parallel, the thermoelectric generating elements are assumed to be insulated, both electrically and thermally, from their surroundings, except at the junction–reservoir contacts. I_g is the current assumed to flow along the arms of the generator, T_1 and T_2 are the temperatures of the hot junction and cold junction respectively, for simplification, T_1 is assumed to be equal to the operating temperature of the DCFC, T, and the temperature of the cold junction, T_2, is assumed to be equal to the temperature of the environment, T_0. When the TEG operates stably, the boundary conditions are determined by $T_1(0) = T_2(0) = \cdots T_i(0) = \cdots = T_m(0) = T$ and $T_1(L) = T_2(L) = \cdots T_i(L) = \cdots = T_m(L) = T_0$, where L is the arm length of the TEG and m is the number of TEG couples. Owing to the fact that there exists a finite temperature difference between the hot and the cold junctions, a heat leak, $K(T-T_0)$, from the hot junction to the cold junction via the semiconductor elements should be considered [34]. Thus, the heat conductions of the TEG

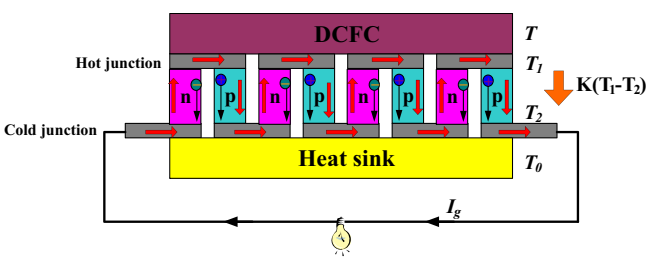

Fig. 2. The schematic diagram of a multi-couple TEG.

between the DCFC and the environment can be, respectively, expressed as follows [35,36]

$$q_1 = \alpha I_g T - 0.5I_g^2R + K(T - T_0), \tag{5}$$

and

$$q_2 = \alpha I_g T_0 + 0.5I_g^2R + K(T - T_0), \tag{6}$$

where $\alpha = (\alpha_p - \alpha_n)m$ is the total Seebeck coefficient, the subscripts "p" and "n" stand for p- and n-type semiconductor legs; $R = (\rho_p l_p/S_p + \rho_n l_n/S_n)m$ is the total electrical resistance of the semiconductor couple, ρ is the electrical resistivity, l is the length of the semiconductor arms, S is the cross-sectional areas of semiconductor arms; I_g^2R represents the Joule heat resulted from the electrical resistance in the TEG; $K = (\kappa_pS_p/l_p + \kappa_nS_n/l_n)m$ is the total thermal conductance of semiconductor couple, κ is the thermally conductivity of the semiconductor materials.

Based on Eqs. (5) and (6), the power output and efficiency of the TEG can be, respectively, expressed as

$$P_{TEG} = q_1 - q_2 = K(T - T_0)j - kJ^2/Z, \tag{7}$$

and

$$\eta_{TEG} = \frac{P_{TEG}}{q_1} = \frac{Z(T - T_0)j - j^2}{Z(T - T_0) + ZTj - j^2/2}, \tag{8}$$

where $j = \alpha I_g/K$ and $Z = \alpha^2/(KR)$ are, respectively, the dimensionless electrical current and the figure of merit of the semiconductor materials [37]. When some heat are transferred from the DCFC DCFC to the TEG, both the power output and the efficiency are larger than zero, i.e., $P_{TEG} > 0$ and $\eta_{TEG} > 0$, and thus one may easily determine the region of the dimensionless electrical current that the TEG takes effect as follows

$$0 < j < Z(T - T_0), \tag{9}$$

where $Z(T - T_0)$ is the maximum dimensionless electrical current allowable for the TEG to generate electricity.

2.4. The efficiency and power output of the hybrid system

As clearly illustrated in Fig. 1, the total heat released in the DCFC is divided into three parts. Besides the part used to replenish the regenerative losses as described by Eq. (4), the part leaked into the environment via convective and/or conductive heat transfer and the part transferred to the TEG for electricity generation can be respectively expressed as

$$q_L = \alpha_L A_L(T - T_0), \tag{10}$$

and

$$\begin{aligned} q_1 &= -\Delta\dot{H} - P_{DCFC} - q_{re} - q_L \\ &= -\frac{A\Delta h}{n_eF}\left[(1 - \eta_{DCFC})J - \frac{n_eFc_1(T - T_0)}{-\Delta h} - \frac{n_eFc_2(T - T_0)}{-\Delta h}\right], \end{aligned} \tag{11}$$

where α_L is the convective and/or conductive heat-leak coefficient, A_L is the heat-transfer area, $c_1 = \alpha_{re}A_{re}(1-\varepsilon)/A$ and $c_2 = \alpha_LA_L/A$ are two constants which are independent of temperature.

By considering the heat leak between the hot and cold junctions, the TEG in the hybrid system begins to exert its function only when the following condition is satisfied:

$$-\Delta\dot{H} - P_{DCFC} > q_{re} + q_L + K(T - T_0). \tag{12}$$

Substituting Eqs. (2), (4) and (10) into Eqs. (11), (12) can be further explicitly rewritten as

$$J > J_C = \left[\frac{n_eF}{-\Delta h(1 - \eta_{DCFC})}\right][(c_1 + c_2)(T - T_0) + K(T - T_0)/A], \tag{13}$$

Table 1
Parameters used in the modeling [24,25,37,29,38].

Parameter	Value
Operating pressure, P (Pa)	1.01325×10^5
Ideal gas constant, R (J/mol K)	8.314
Faraday constant, F (C/mol)	96,485
Height of packed bed anode, H (m)	1.0×10^{-3}
Number of electrons involved per reaction, n_e	4
Polar plate area of a DCFC, A (m^2)	0.04
Diameter of spherical graphite particle, D_c (m)	1.0×10^{-5} [24,25]
Concentration independent cathode exchange current density, $j^0_{0,cat}$ (A/m^2)	5.0×10^2 [25]
Pre-exponential factor of the backward reaction, K_B (A/m^2)	5.8×10^9 [29]
Temperature activation of the backward reaction, E_B (K^{-1})	22,175 [29]
Mass transport coefficient of CO_2, K_{CO_2} (m/s)	3.5×10^{-2} [25]
Constant, r_1	−1.250 [24,25]
Constant, r_2	0.375 [25]
Bulk gas compositions at the cathode side	67%CO_2/33% O_2 [25]
Operating temperature of DCFC, T (K)	923
Temperature of environment, T_0 (K)	298
Constant c_1 ($W\,m^{-2}\,K^{-1}$)	0.1
Constant c_2 ($W\,m^{-2}\,K^{-1}$)	0.1
Figure of merit of the semiconductor materials, ZT_0	1.0 [37]
Heat conductivity, K ($W\,K^{-1}\,m^{-1}$)	1.5×10^{-2} [38]

where J_C is the critical operating current density of the DCFC from which the TEG in the hybrid system starts to work.

When $J > J_C$ and $0 < j < Z(T - T_0)$, the fundamental relationship between the operating current density of the DCFC, J, and the dimensionless current of the TEG, j, is given by the following equation:

$$j^2 - 2ZTj - 2Z(T - T_0) + \frac{2ZA}{K}\left[\frac{-\Delta h}{n_e F}(1 - \eta_{DCFC})J - (c_1 + c_2)(T - T_0)\right] = 0. \quad (14)$$

Combining Eqs. (9) and (14), one may easily determine the maximum operating current density of the DCFC, J_M, from which the TEG in the hybrid system stops working. Thus, the TEG in the hybrid system cannot take effects in the entire operating current density region of DCFC but only works in the following region

$$J_C < J < J_M. \quad (15)$$

When $J_C < J < J_M$, based on Eqs. (2), (3), (7) and (8), the numerical expressions of the power output and efficiency of the hybrid system can be, respectively, expressed as

$$P = P_{DCFC} + P_{TEG} = VJA + KT_0[(T/T_0 - 1)j - j^2/(ZT_0)], \quad (16)$$

and

$$\eta = \frac{P_{DCFC} + P_{TEG}}{-\Delta \dot{H}} = \eta_{DCFC} + \frac{n_e F K T_0[(T/T_0 - 1)j - j^2/(ZT_0)]}{-JA\Delta h}. \quad (17)$$

When $J \leqslant J_C$ or $J \geqslant J_M$, the power output and efficiency of the hybrid system equal to that of the sole DCFC, i.e.,

$$P = P_{DCFC}, \quad (18)$$

and

$$\eta = \eta_{DCFC}. \quad (19)$$

It is worthwhile to mention that J and j in Eqs. (16) and (17) are not independent of each other, and the relationship between J and j is given by Eq. (14).

3. Results and discussion

As shown by Eqs. (16)–(19), the performance of the TEG-based DCFC hybrid system not only depends on the parameters related to the DCFC such as operating temperature, operating current density, electrolyte thickness, but also depends on the parameters related to the TEG such as electrical resistance and thermal conductance, figure of merit of the thermoelectric materials, geometric parameters and so on. In the following, numerical calculations are carried out by using the commercial software MATLAB® based on the mathematical model developed in Section 2 and the parameters summarized in Table 1, and these parameters are taken as default values unless specifically mentioned.

The power densities and efficiencies of the DCFC, TEG and hybrid system varying with the operating current density of the DCFC are clearly shown in Fig. 3, where $P^* = P/A$ is the power density, P^*_{max} is the maximum power density, and J_P is the operating current density corresponding to P^*_{max}. Fig. 3(a) shows that the state of the hybrid system at the maximum power output is different from that of the DCFC or TEG at the maximum power output. It is also observed that the power density of the hybrid system first increases and then decreases as the operating current density is increased, while the efficiency first rapidly decreases then slightly

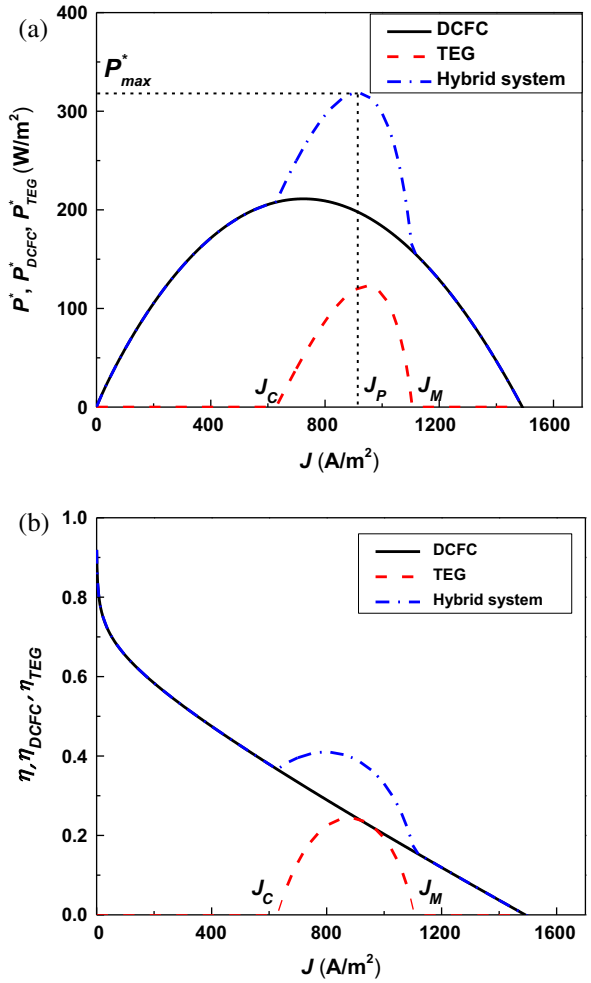

Fig. 3. The curves of (a) power densities and (b) efficiencies of the DCFC, TEG, and hybrid system varying with the operating current density of the DCFC, where $P^* = P/A$ is the power density of the hybrid system, P^*_{DCFC} and P^*_{TEG} are the power densities of the DCFC and TEG, J_P is the current density corresponding to the maximum power density of the hybrid system P^*_{max}.

increases and finally decreases as the operating current density increases. The intermediate slightly augment in the efficiency occurs in the region of $J_C < J < J_M$ because the increase in the efficiency contributed by the TEG is larger than the decrease in efficiency caused by the DCFC. When $0 < J \leqslant J_C$ or $J \geqslant J_M$, the curves of the power density and efficiency of the hybrid system are overlapped with that of the sole DCFC. When $J_C < J < J_M$, the power density and efficiency of the hybrid system are larger than either that of the DCFC or that of the TEG. It clearly shows that the performance can be effectively enhanced by coupling a TEG to the DCFC for further converting the waste heat into power generation in specific operation conditions, and the increase in the power density is more significantly than that in the efficiency. For the typical parameters given in Table 1, the maximum power density of the hybrid system is 318.46 W m^{-2}, which is about 50.81% larger than that of the sole DCFC, 211.16 W m^{-2}. Meanwhile, the efficiencies of the hybrid system and DCFC corresponding to the their maximum power densities are, respectively, 38.63% and 32.30%, and the efficiency of the hybrid system is about 19.60% larger than that of the sole DCFC.

It is seen from Figs. 4 and 5 that the power density and efficiency of the hybrid system are affected by the operating temperature of the DCFC, T, and the thermal conductance of the TEG, K. When $J \leqslant J_C$ or $J \geqslant J_M$, the efficiency and power density of the hybrid system are increased with the increasing operating temperature T, while the efficiency and power density are the same as that

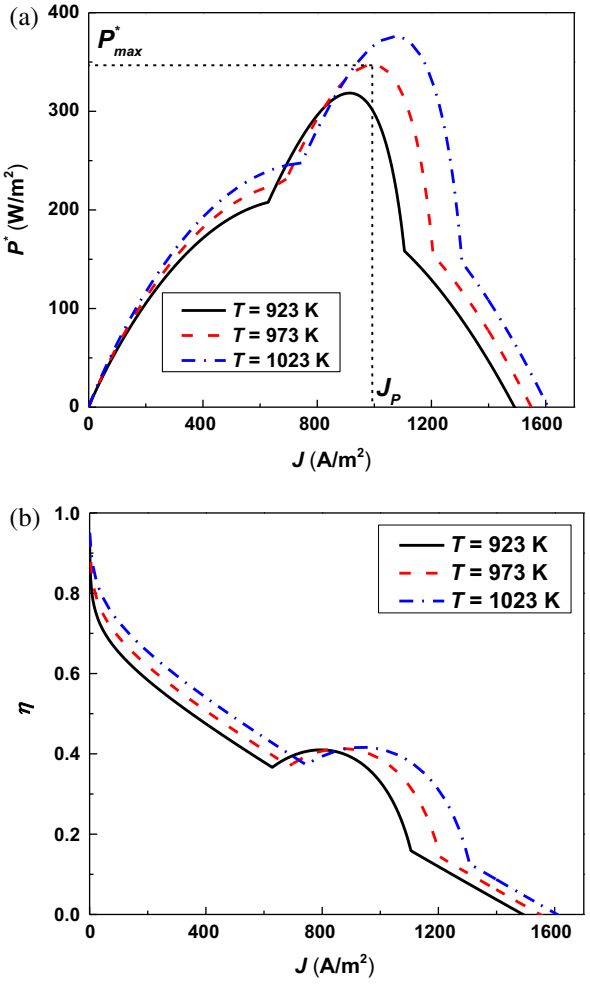

Fig. 4. The effects of operating temperature T on the (a) power density, and (b) efficiency of the hybrid system.

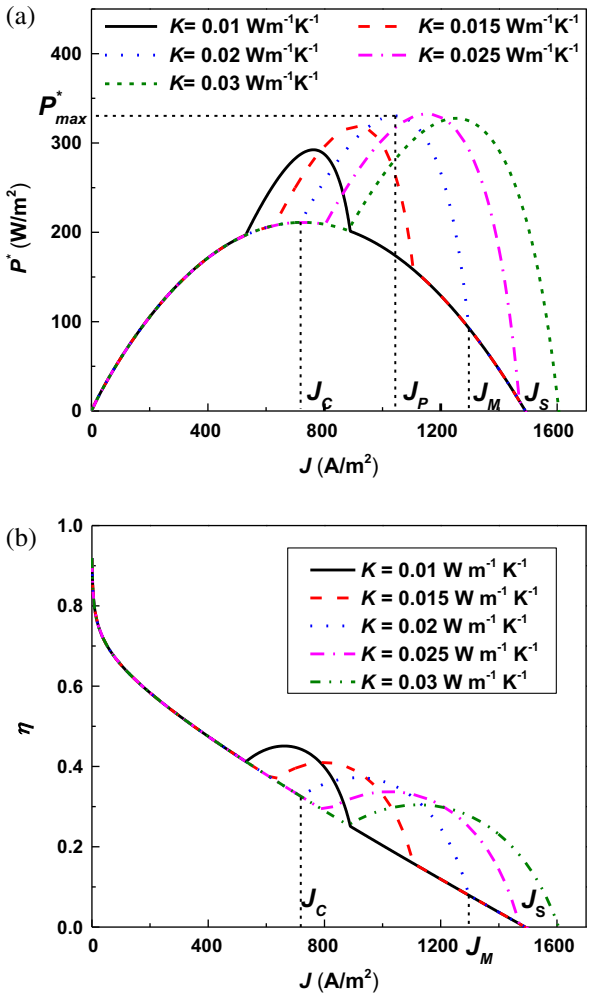

Fig. 5. The effects of heat conductivity K on the (a) power density, and (b) efficiency of the hybrid system, where J_S is the stagnation current density that the DCFC .

of the sole DCFC for different thermal conductance K. The values of J_C, J_M and J_P shift to larger ones as the operating temperature T or thermal conductance K is increased, and J_P is usually located between J_C and J_M. The effective operating current density interval $\Delta J (= J_M - J_C)$ increases and moves backward as the operating temperature T or the thermal conductance K is increased. It is also seen from Fig. 5(a) that there is an optimum value of the thermal conductance K at which the maximum power density can be attained. For the typical parameters given in Table 1, the optimum value of K is found to be between 0.02 W K^{-1} m^{-1} and 0.03 W K^{-1} m^{-1}. Based on numerical calculations, more detailed values of J_C, J_M, ΔJ, J_P and P^*_{max} under different operating temperature T and thermal conductance K are listed in Table 2. Statistical analysis may be further used to optimize the designing and operating parameters if some proper optimization objectives and more numerical calculation examples are given. Combined Table 2 and Figs. 4 and 5, it is interesting to note that the power density and efficiency of the hybrid system will be still larger than zero even when the operating current density is larger than the stagnation current density J_S that the DCFC does not contribute any more. For this case, the DCFC in the hybrid system is operated as a high-temperature heat source more than an electrochemical converter.

The influences of the integrated parameters c_1 and c_2 on the performance of the hybrid system are clearly shown in Fig. 6. It is observed from Fig. 6 that the influence of c_1 is only occurred in the region of $J_C < J < J_M$, the power density and efficiency will

Table 2
The values of j_C, j_M, j_P and P^*_{max} for different operating temperature T and thermal conductance K, where c_1 = 0.1 W m^{-2} K^{-1} and c_2 = 0.1 W m^{-2} K^{-1}.

T (K)	K (W K^{-1} m^{-1})	J_C (A/m^2)	J_M (A/m^2)	$\Delta J = J_M - J_C$ (A/m^2)	J_P (A/m^2)	P^*_{max} (W/m^2)
923	0.01	530	888	358	762	292.4
	0.015	628	1105	477	913	318.5
	0.02	719	1296	577	1040	330.3
	0.025	803	1469	666	1152	332.6
	0.03	882	1629	747	1252	327.7
973	0.01	582	974	392	832	322.0
	0.015	686	1205	519	992	347.3
	0.02	782	1409	627	1126	357.3
	0.025	870	1593	723	1243	356.9
	0.03	954	1763	809	1348	349.1
1023	0.01	635	1060	425	903	351.7
	0.015	745	1306	561	1071	375.9
	0.02	845	1522	677	1212	383.7
	0.025	938	1717	779	1334	380.6
	0.03	1025	1897	872	1443	369.5

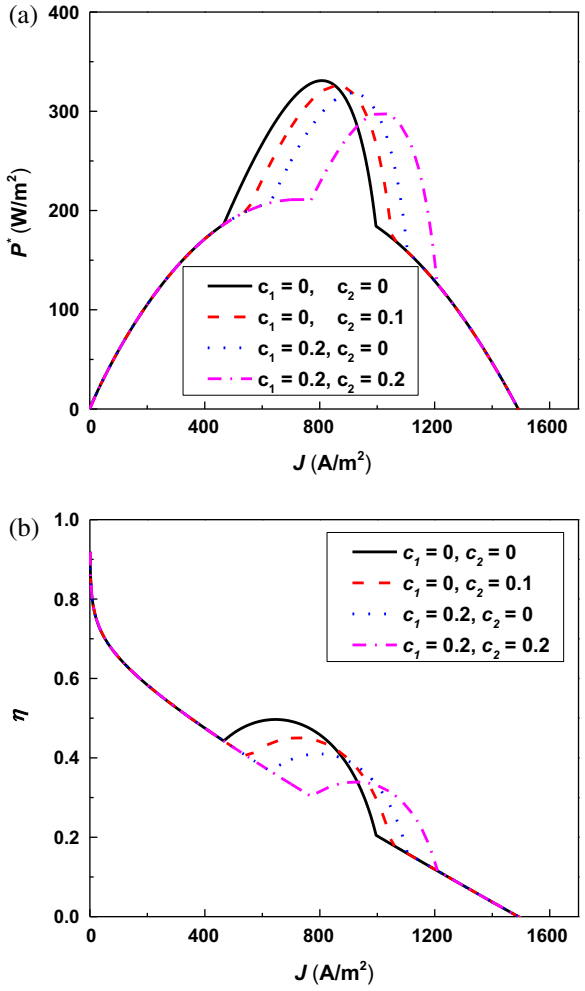

Fig. 6. The effects of integrated parameters c_1 and c_2 on the (a) power density, and (b) efficiency of the hybrid system, where the units of c_1 and c_2 are W m^{-2} K^{-1}.

decrease as the parameter c_1 increases, while the current densities J_C, J_M, and J_P will increase as the parameter c_1 is increased. When the regenerative losses in the regenerator are negligible, i.e., $c_1 = 0$, the fundamental relationship between the operating current density of the DCFC and the dimensionless current of the TEG can be reduced from Eq. (14) to

$$j^2 - 2ZTj - 2Z(T - T_0) + \frac{2ZA}{K}\left[\frac{-\Delta h}{n_e F}(1 - \eta_{DCFC})J - c_2(T - T_0)\right] = 0. \quad (20)$$

For this case, the curves of the power density and efficiency varying with the operating current density are shown by the red dash curve in Fig. 6.

Similar to the effect of parameter c_1, the influence of the integrated parameter c_2 on the performance of the hybrid system is also only occurred in the region of $J_C < J < J_M$, the power density and efficiency will decrease with the increasing parameter c_2, while the current densities J_C, J_M, and J_P will increase as the parameter c_2 is increased. When the heat-leak from the DCFC to the environment is negligible, i.e., $c_2 = 0$, the fundamental relationship between the operating current density of the DCFC and the dimensionless current of the TEG can be reduced from Eq. (14) to

$$j^2 - 2ZTj - 2Z(T - T_0) + \frac{2ZA}{K}\left[\frac{-\Delta h}{n_e F}(1 - \eta_{DCFC})J - c_1(T - T_0)\right] = 0. \quad (21)$$

For this case, the curves of the power density and efficiency varying with the operating current density are shown by the blue dot curve in Fig. 6.

When both the heat-leak from the DCFC to the environment and the regenerative losses in the regenerator are negligible, i.e., $c_1 = 0$ and $c_2 = 0$, the fundamental relationship between the operating current density of the DCFC and the dimensionless current of the TEG can be reduced from Eq. (14) to

$$j^2 - 2ZTj - 2Z(T - T_0) + \frac{2ZA}{K}\left[\frac{-\Delta h}{n_e F}(1 - \eta_{DCFC})J\right] = 0. \quad (22)$$

For this case, the curves of the power density and efficiency varying with the operating current density are shown by the black solid curve in Fig. 6.

4. Conclusions

A DCFC–TEG hybrid system mainly composed of a DCFC, a multi-couple TEG and a regenerator has been proposed to effectively recover the waste heat generated in the DCFC. By considering the main thermodynamic–electrochemical irreversibilities, the analytical expressions of performance parameters for the hybrid system are derived, from which the general performance characteristics are revealed. The operating current density interval of the DCFC that the TEG exerts its function is determined. It is found that the performance of the DCFC can be significantly improved by coupling a TEG to the DCFC for additional electricity generation, and the increase in the power density is more significantly than that in the efficiency. The influences of the operating current density and operating temperature of the DCFC, thermal conductance of the TEG, and two integrated parameters c_1 and c_2 on the performance of the hybrid system are discussed. The results obtained in the paper may offer some theoretical guidance for the performance improvement of DCFCs through cogeneration systems.

Acknowledgments

This work has been supported by the National Natural Science Foundation of China (Grant No. 51406091), the Natural Science Foundation of Zhejiang Province of China (Grant No. LQ14E06002), the Natural Science Foundation of Ningbo City (Grant Nos. 2013A610139, 2013A610033), the Foundation of Zhejiang Educational Commission (Grant Nos. Y201326937, Y201326905, Y201430419), the Zhejiang Open Foundation of the Most Important

Subjects (Grant No. xkzw108), and the K.C. Wong Magna Fund in Ningbo University.

References

[1] Nürnberger S, Bubar R, Desclaux P, Franke B, Rzepka M, Stimming U. Direct carbon conversion in a SOFC-system with a non-porous anode. Energy Environ Sci 2010;3:150–3.
[2] Li X, Zhu Z, De Marco R, Bradley J, Dicks A. Evaluation of raw coals as fuels for direct carbon fuel cells. J Power Sources 2010;195:4051–8.
[3] Chen W, Xu R. Clean coal technology development in China. Energy Policy 2010;38:2123–30.
[4] Liu R, Zhao C, Li J, Zeng F, Wang S, Wen T, et al. A novel direct carbon fuel cell by approach of tubular solid oxide fuel cells. J Power Sources 2010;195:480–2.
[5] Hao W, He X, Mi Y. Achieving high performance in intermediate temperature direct carbon fuel cell with renewable carbon as a fuel source. Appl Energy 2014;135:174–81.
[6] Yu J, Zhao Y, Li Y. Utilization of corn cob biochar in a direct carbon fuel cell. J Power Sources 2014;270:312–7.
[7] Giddey S, Badwal SPS, Kulkarni A, Munnings C. A comprehensive review of direct carbon fuel cell technology. Prog Energy Comb Sci 2012;38:360–99.
[8] Hackett GA, Zondlo JW, Svensson R. Evaluation of carbon materials for use in a direct carbon fuel cell. J Power Sources 2007;168:111–8.
[9] Li S, Lee AC, Mitchell RE, Gür TM. Direct carbon conversion in a helium fluidized bed fuel cell. Solid State Ionics 2008;179:1549–52.
[10] Jia L, Tian Y, Liu Q, Xia C, Yu J, Wang Z, et al. A direct carbon fuel cell with (molten carbonate)/(doped ceria) composite electrolyte. J Power Sources 2010;195:5581–6.
[11] Liu R, Zhao C, Li J, Zeng F, Wang S, Wen T, et al. A novel direct carbon fuel cell by approach of tubular solid oxide fuel cells. J Power Sources 2010;195:480–2.
[12] Jain SL, Lakeman JB, Pointon KD, Marshall R, Irvine JTS. Electrochemical performance of a hybrid direct carbon fuel cell powered by pyrolysed MDF. Energy Environ Sci 2009;2:687–93.
[13] Kulkarni A, Giddey S, Badwal SPS, Paul G. Electrochemical performance of direct carbon fuel cells with titanate anodes. Electrochim Acta 2014;121:34–43.
[14] Lee EK, Chun HH, Kim YT. Enhancing Ni anode performance via Gd_2O_3 addition in molten carbonate-type direct carbon fuel cell. Int J Hydrogen Energy 2014;39:16541–7.
[15] Steinberg M. Conversion of fossil and biomass fuels to electric power and transportation fuels by high efficiency integrating plasma fuel cell (IPFC) energy cycle. Int J Hydrogen Energy 2006;31:405–11.
[16] Liu Q, Tian Y, Li H, Jia L, Xia C, Thompson LT, et al. High efficiency chemical energy conversion system based on a methane catalytic decomposition reaction and two fuel cells: Part I. Process modeling and validation. J Power Sources 2010;195:6539–48.
[17] Liu Q, Tian Y, Li H, Jia L, Xia C, Thompson LT, et al. High efficiency chemical energy conversion system based on a methane catalytic decomposition reaction and two fuel cells: Part II. Exergy analysis. J Power Sources 2010;195:6532–8.
[18] Ali H, Sahin AZ, Yilbas BS. Thermodynamic analysis of a thermoelectric power generator in relation to geometric configuration device pins. Energy Convers Manage 2014:634–40.
[19] Sahin AZ, Yilbas BS. The thermoelement as thermoelectric power generator: effects of leg geometry on the efficiency and power generation. Energy Convers Manage 2013;65:26–32.
[20] Gou X, Yang S, Xiao H, Ou Q. A dynamic model for thermoelectric generator applied in waste heat recovery. Energy 2013;52:201–9.
[21] Zheng XF, Yan YY, Simpson K. A potential candidate for the sustainable and reliable domestic energy generation–thermoelectric cogeneration system. Appl Therm Eng 2013;53:305–11.
[22] Yamashita O. Effect of linear and non-linear components in the temperature dependences of thermoelectric properties on the energy conversion efficiency. Energy Convers Manage 2014;78:634–40.
[23] Wang Y, Dai C, Wang S. Theoretical analysis of a thermoelectric generator using exhaust gas of vehicles as heat sources. Appl Energy 2014;112:1171–80.
[24] Liu Q, Tian Y, Xia C, Thompson LT, Liang B, Li Y. Modeling and simulation of a single direct carbon fuel cell. J Power Sources 2008;185:1022–9.
[25] Zhang H, Chen L, Zhang J, Chen J. Performance analysis of a direct carbon fuel cell with molten carbonate electrolyte. Energy 2014;68:292–300.
[26] Bockris JO, Kim J. Effect of contact resistance between particles on the current distribution in a packed bed electrode. J Appl Electrochem 1997;27:890–901.
[27] Zhao Y, Chen J. Modeling and optimization of a typical fuel cell-heat engine hybrid system and its parametric design criteria. J Power Sources 2009;186:96–103.
[28] Zhang H, Lin G, Chen J. Performance analysis and multi-objective optimization of a new molten carbonate fuel cell system. Int J Hydrogen Energy 2011;36:4015–21.
[29] Elleuch A, Boussetta A, Halouani K. Analytical modeling of electrochemical mechanisms in CO_2 and CO/CO_2 producing direct carbon fuel cell. J Electroanal Chem 2012;668:99–106.
[30] Prins-Jansen JA, Hemmes K, De Wit JHW. An extensive treatment of the agglomerate model for porous electrodes in molten carbonate fuel cells-I. Qualitative analysis of the steady-state model. Electrochim Acta 1997;42:3585–600.
[31] Arato E, Bosio B, Costa P Parodi F. Preliminary experimental and theoretical analysis of limit performance of molten carbonate fuel cell. J Power Sources 2001;102:74–81.
[32] Zhang H, Lin G, Chen J. Performance evaluation and parametric optimum criteria of an irreversible molten carbonate fuel cell-heat engine hybrid system. Int J Electrochem Sci 2011;6:4714–29.
[33] Chen L, Zhang H, Gao S, Yan H. Performance optimum analysis of an irreversible molten carbonate fuel cell-stirling heat engine hybrid system. Energy 2014;64:923–30.
[34] Chen J, Andresen B. New bounds on the performance parameters of a thermoelectric generator. Int J Power Energy Sys 1997;17:23–7.
[35] Chen J, Lin B, Wang H, Lin G. Optimal design of a multi-couple thermoelectric generator. Semicond Sci Technol 2000;15:184–8.
[36] Chen X, Chen L, Guo J, Chen J. An available method exploiting the waste heat in a proton exchange membrane fuel cell system. Int J Hydrogen Energy 2011;36:6099–104.
[37] Chen X, Pan Y, Chen J. Performance and evaluation of a fuel cell-thermoelectric generator hybrid system. Fuel Cells 2010;10:1164–70.
[38] Chen L, Sun F, Wu C. Thermoelectric-generator with linear phenomenological heat-transfer law. Appl Energy 2005;81:358–64.